

Single-Channel Tissue Segmentation via Cross-Modal Distillation from Foundation Models

1st Sakib Mohammad

Department of Engineering Technology
Fairmont State University
Fairmont, WV, USA
smohammad@fairmontstate.edu

2nd Jarin Ritu

Department of Electrical and Computer
Engineering
Texas A&M University
College Station, TX, USA
jarin.ritu@tamu.edu

3rd Md Sakhawat Hossain

Department of Mechanical Engineering
Auburn University
Auburn, AL, USA
mdh0127@auburn.edu

Abstract—Multiplexed fluorescence microscopy improves tissue segmentation by providing complementary channels including nuclear (DAPI) and membrane (E-cadherin), that together encode richer spatial context than single-channel imaging alone. However, multiplexed models require all channels at inference, limiting deployment where only a subset is available. This work proposes a cross-modal knowledge distillation framework that transfers semantic information from a frozen foundation model teacher processing multiplexed input to a lightweight student operating on the nuclear channel only. The distillation objective combines MSE-based probability matching, boundary-aware supervision, and learnable uncertainty weighting. SAM ViT-H and CellSAM are evaluated as teachers across four U-Net students: Swin-Tiny (27M), ResNet18 (11M), EfficientNet-B0 (5.3M), and MobileNetV3 (1.5M), on TissueNet and BBBC038. On TissueNet, the SAM-distilled Swin-Tiny student achieves Dice 78.36 (± 1.44), a 13.05-point improvement over the no-KD baseline (65.31 ± 1.35) and 87.9% recovery of teacher oracle performance (89.12 ± 1.21) at a $23\times$ parameter reduction. KD consistently improves all four students by ~ 12 Dice points, confirming architecture-agnostic distillation. SAM ViT-H outperforms CellSAM as teacher across all settings. Cross-dataset evaluation on BBBC038 shows consistent gains without teacher retraining.

Index Terms—tissue segmentation, knowledge distillation, foundation models, multiplexed imaging, single-channel inference, missing-channel constraints

I. INTRODUCTION

Accurate segmentation of tissues and cells is a fundamental task in biomedical image analysis, supporting applications such as disease characterization, spatial profiling, and quantitative pathology [1]. Despite significant advances in deep learning based segmentation [2], accurate delineation of cell boundaries remains challenging due to variations in cell morphology, imaging modalities, and tissue heterogeneity [3]. Recent advances in multiplexed imaging have enabled the acquisition of high dimensional data where multiple image channels capture complementary biological features within a single sample, for example, nuclear staining (DAPI) and membrane markers (E-cadherin) that together provide a richer

spatial context than either channel alone. Models trained on such representations consistently outperform single-channel counterparts on segmentation benchmarks [3].

However, multiplexed imaging increases memory use, latency, and model complexity, limiting scalability in resource-constrained settings. It also requires all channels at inference, which may be impractical in real-life scenarios where only a single channel may be available. These constraints motivate methods that can reduce input dimensionality while preserving the semantic information encoded in multiplexed representations. Knowledge distillation (KD) [4] offers a principled solution: a large teacher model trained on high dimensional inputs transfer implicit knowledge to a compact student model. While KD has been widely applied to model compression in classification [4] and semantic segmentation [5], its application to *cross-modal* distillation, where the teacher and student operate on inputs of different dimensionality, remains largely unexplored, particularly in biomedical imaging.

In this work, we propose a cross-modal KD framework that transfers semantic information from multiplexed microscopy images to single-channel inputs for tissue segmentation. A frozen foundation-model teacher processes nuclear and membrane channels and generates soft-targets to guide a lightweight student trained only on the nuclear channel. We evaluate two teachers: Segment Anything Model (SAM) [6] with a ViT-H [7], and CellSAM [8], and four U-Net [2] encoder backbones: Swin-Tiny [9], ResNet18 [10], EfficientNet-B0 [11], and MobileNetV3 [12]. The framework is further assessed on BBBC038 [13] to examine cross-dataset generalization without teacher retraining. The main contributions of this work are as follows:

- Cross-modal knowledge distillation that transfers semantic information from a frozen multiplexed foundation model teacher to a lightweight single-channel student for tissue segmentation under missing-channel settings
- An uncertainty-weighted distillation objective that inte-

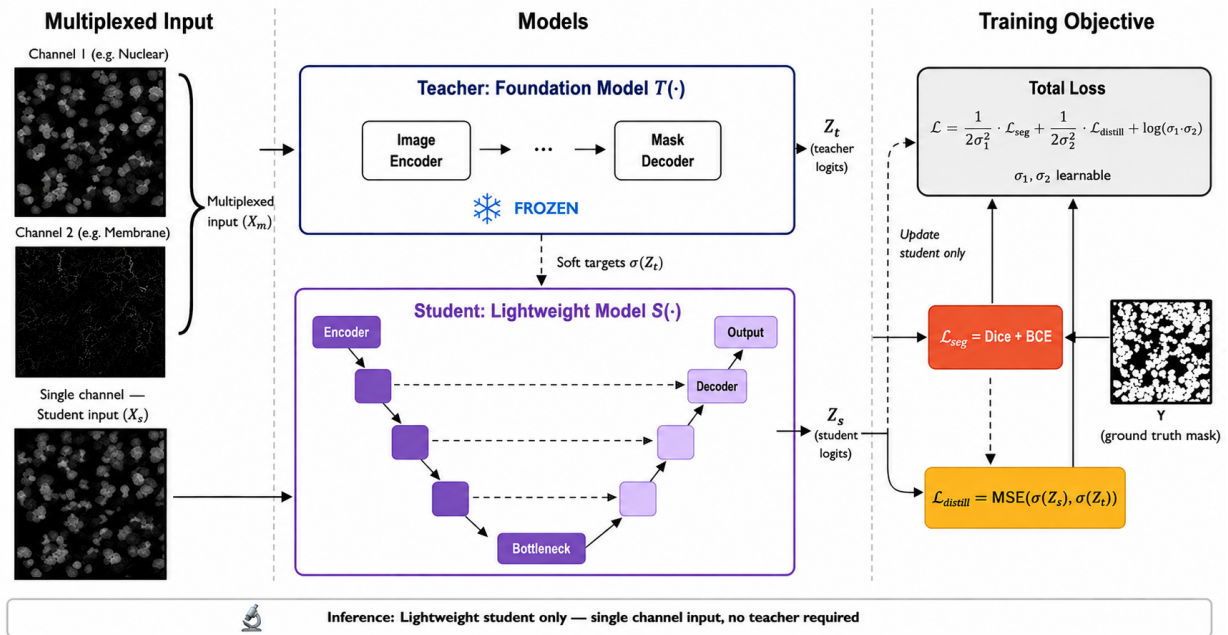


Fig. 1. Overview of the proposed cross-modal knowledge distillation framework. A frozen foundation model teacher $T(\cdot)$ processes multiplexed images X_m and generates soft targets $\sigma(Z_t)$. A lightweight student model $S(\cdot)$ is trained on single-channel input X_s using a combination of segmentation loss \mathcal{L}_{seg} , distillation loss $\mathcal{L}_{distill}$, and learnable uncertainty weights σ_1, σ_2 [14]. At inference, only the student is deployed — no teacher or multiplexed input is required.

grates soft-target matching and boundary-aware supervision to balance heterogeneous training signals

- Extensive evaluation of SAM ViT-H and CellSAM teachers with four student architectures on TissueNet and BBBC038, achieving consistent performance improvements and up to $421\times$ parameter reduction
- A cross-dataset distillation protocol that leverages TissueNet teacher predictions to supervise students trained exclusively on BBBC038, without teacher retraining or target-domain multiplexed data

A. Related Work

1) *Biomedical Image Segmentation*: Deep learning has substantially advanced cell and tissue segmentation, with U-Net [2] becoming a standard architecture due to its encoder-decoder design and skip connections. More recent approaches have incorporated transformer-based encoders such as Swin Transformer [9] and lightweight backbones including MobileNet [15] and EfficientNet [11]. Large-scale benchmarks such as TissueNet [3] have further shown that combining nuclear and membrane channels improves segmentation performance over single-channel imaging, motivating the transfer of multiplexed information to single-channel models.

2) *Foundation Models for Segmentation*: Foundation models have recently demonstrated strong zero-shot segmentation capabilities. SAM [6] established a general-purpose segmentation framework, while MedSAM [16] and CellSAM [8] adapted these capabilities to medical and cellular imaging domains. Although these models achieve strong segmentation performance, they typically require the same input modalities

available during training and inference. In this work, SAM and CellSAM are used as frozen teachers to transfer multiplexed information to single-channel students.

3) *Knowledge Distillation*: Knowledge distillation (KD) [4] transfers knowledge from a high-capacity teacher to a compact student using soft prediction targets and has been widely applied to model compression in classification and dense prediction tasks [5]. Recent studies have explored distilling foundation models into lightweight task-specific networks; however, most assume that teacher and student operate on the same input modality. Cross-modal KD between multiplexed and single-channel biomedical images remains largely unexplored. The proposed framework addresses this gap through cross-modal distillation combined with uncertainty-weighted optimization [14].

II. METHODOLOGY

The proposed cross-modal knowledge distillation framework is illustrated in Fig. 1. The teacher, a frozen foundation model, processes multiplexed images containing nuclear and membrane channels, generating pixel-wise soft probability targets. The student, a lightweight encoder-decoder network, is trained exclusively on the single nuclear channel, supervised jointly by the ground truth mask and the teacher’s soft targets. At inference, only the student is deployed with no dependency on the teacher or multiplexed data.

A. Problem Formulation

Let $X_m \in \mathbb{R}^{H \times W \times C}$ denote the multiplexed image with C channels, $X_s \in \mathbb{R}^{H \times W \times 1}$ the single-channel counterpart, and

$Y \in \{0, 1\}^{H \times W}$ the binary segmentation mask. The objective is to learn a student model $S(\cdot)$ operating exclusively on X_s that achieves segmentation performance comparable to a teacher model $T(\cdot)$ with access to the full multiplexed input X_m . This is formulated as cross-modal KD, where the student learns from both ground truth masks and teacher outputs to transfer semantic information from the high-dimensional multiplexed space into a single-channel representation.

B. Distillation Objective

The teacher $T(\cdot)$ processes multiplexed input X_m and produces pixel-wise logits $Z_t = T(X_m) \in \mathbb{R}^{H \times W}$, which are cached to disk prior to student training. The student $S(\cdot)$ processes single-channel input X_s and produces logits $Z_s = S(X_s) \in \mathbb{R}^{H \times W}$. KD is performed by aligning the pixel-wise sigmoid probabilities of the teacher and student. Rather than temperature-scaled KL divergence as in classification KD [4], MSE between sigmoid probabilities is employed, which is better suited to binary single-logit segmentation outputs:

$$\mathcal{L}_{distill} = \frac{1}{HW} \sum_{i=1}^{HW} (\sigma(Z_t^i) - \sigma(Z_s^i))^2 \quad (1)$$

where $\sigma(\cdot)$ is the sigmoid function. This formulation directly minimizes pixel-wise probability discrepancy between teacher and student, providing a smooth and stable training signal.

C. Segmentation and Boundary Losses

The supervised segmentation loss combines binary cross-entropy and Dice loss to jointly optimize pixel-wise accuracy and overlap under class imbalance:

$$\mathcal{L}_{seg}^{(S)} = \mathcal{L}_{BCE}(S(X_s), Y) + \mathcal{L}_{Dice}(S(X_s), Y) \quad (2)$$

Cell boundary pixels are critical for downstream morphological analysis and represent the regions where nuclear-only models most frequently fail. A boundary-aware loss \mathcal{L}_{bnd} concentrates gradient signal at these locations. The boundary mask M_{bnd} is obtained by subtracting the morphologically eroded ground truth from the original mask:

$$\mathcal{L}_{bnd} = \mathcal{L}_{BCE}(S(X_s) \odot M_{bnd}, Y \odot M_{bnd}) \quad (3)$$

where \odot denotes element-wise multiplication.

D. Overall Objective Function

Balancing segmentation, distillation, and boundary objectives requires careful loss weighting. Rather than fixed coefficients, learnable uncertainty weighting [14] is employed to automatically determine the optimal balance during training, eliminating manual hyperparameter tuning. The total loss is defined as:

$$\mathcal{L}_{total} = \frac{1}{2\sigma_1^2} \mathcal{L}_{seg}^{(S)} + \frac{1}{2\sigma_2^2} \mathcal{L}_{distill} + \beta \mathcal{L}_{bnd} + \log(\sigma_1 \cdot \sigma_2) \quad (4)$$

where σ_1 and σ_2 are learnable scalar parameters optimized jointly with the student weights. Scaling each loss term inversely with its associated uncertainty σ_i^2 places more weight on objectives where the model is more confident, while the logarithmic regularization term prevents the trivial solution of $\sigma_1, \sigma_2 \rightarrow \infty$. The boundary loss weight $\beta = 0.3$ is fixed, as boundary pixels constitute a small fraction of the image and excessive boundary weighting can destabilize training.

E. Training Procedure

Training proceeds in two stages. In the first stage, the teacher processes all training images and caches pixel-wise soft predictions $\sigma(Z_t)$ to disk. This decouples teacher inference from student training, eliminates the memory cost of loading both models simultaneously, and reduces training time by approximately $4\times$ compared to live teacher inference. In the second stage, the student is trained on single-channel inputs X_s with supervision from both cached soft targets and ground truth masks Y , according to Eq. (4). The learnable parameters σ_1 , σ_2 , and all student weights are optimized jointly. The same two-stage procedure and distillation objective are applied identically across all evaluated student architectures; only the encoder backbone varies between experiments.

F. Cross-Dataset Generalization

To evaluate robustness under distribution shift, TissueNet-cached teacher predictions are used to supervise students trained exclusively on BBBC038 [13], without teacher retraining or target-domain multiplexed data. This reflects realistic deployment conditions where multiplexed reference data from the target domain may be unavailable. The cross-dataset setting is evaluated across all four student architectures to assess whether generalization is consistent across model capacities.

III. EXPERIMENTAL SETUP

A. Datasets

Experiments are conducted on two fluorescence microscopy datasets with different imaging conditions and channel availability. Representative samples are shown in Fig. 2.

TissueNet [3] is a large-scale benchmark containing paired nuclear (DAPI) and membrane channels with corresponding segmentation masks across diverse tissue types. It serves as the primary benchmark, where the teacher receives multiplexed input X_m and the student uses only the nuclear channel X_s at both training and inference.

BBBC038 [13] (Kaggle 2018 Data Science Bowl) contains 670 single-channel nuclear fluorescence images from diverse biological contexts. It is used for cross-dataset evaluation, where TissueNet-cached teacher predictions supervise students trained on BBBC038 without teacher retraining, using an 85/15 fixed-seed train-test split.

B. Preprocessing

All images are center-cropped to 448×448 pixels. Each channel is independently normalized by clipping to the 1st and 99th intensity percentiles and rescaling to $[0, 1]$ [3].

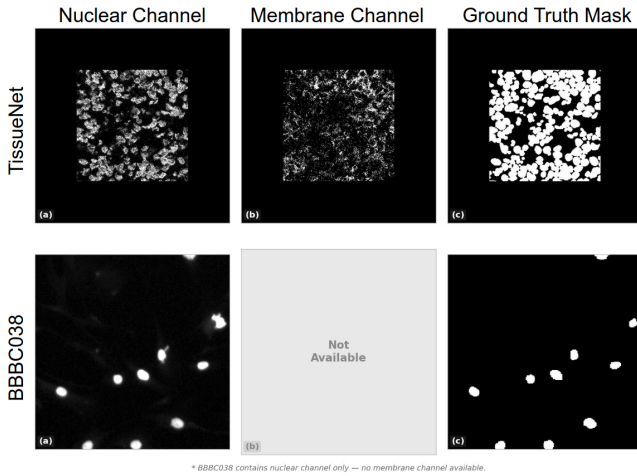


Fig. 2. Representative samples from both datasets. *Top*: TissueNet provides paired nuclear (a) and membrane (b) channels with a binary segmentation mask (c). *Bottom*: BBBC038 contains nuclear channel only — membrane channel is unavailable (b). The teacher receives both TissueNet channels; the student receives only the nuclear channel from either dataset.

For BBBC038, RGB images are first converted to grayscale using standard luminance weights [17]. Training images are augmented with random horizontal and vertical flips and 90° rotations. No augmentation is applied at validation or inference.

C. Models

The framework is teacher-agnostic and can be paired with any foundation model that processes multiplexed inputs and produces pixel-wise predictions. Two frozen zero-shot teachers are evaluated: SAM ViT-H [6] (632M) and CellSAM [8] (635M). Students follow a U-Net architecture with ImageNet-pretrained encoders adapted to single-channel input. Four backbones are considered: Swin-Tiny (27M), ResNet18 (11M), EfficientNet-B0 (5.3M), and MobileNetV3 (1.5M). During inference, only the student and the nuclear channel are required, achieving up to 421× parameter reduction.

D. Implementation Details

Models are implemented in PyTorch and PyTorch Lightning [18]. Students are trained for 50 epochs using AdamW [19] with a learning rate of 3×10^{-5} , 5% linear warmup, cosine annealing decay, and gradient clipping of 0.5. Early stopping with a patience of 10 epochs is applied based on validation Dice. A batch size of 4 and mixed-precision (FP16) training are used throughout. All experiments are conducted on a single NVIDIA A100 GPU (80 GB).

E. Evaluation Metrics

Segmentation performance is measured using Dice coefficient and Intersection-over-Union (IoU):

$$\text{Dice} = \frac{2|P \cap Y|}{|P| + |Y|}, \quad \text{IoU} = \frac{|P \cap Y|}{|P \cup Y|} \quad (5)$$

where P is the predicted mask and Y the ground truth. Results are reported as mean \pm standard deviation over three independent runs, expressed as percentages.

F. Experimental Protocol

Experiments evaluate teacher upper bounds, single-channel student baselines, knowledge-distilled students, and cross-dataset generalization. SAM ViT-H and CellSAM are first evaluated on multiplexed TissueNet inputs. Students are then trained on the nuclear channel with and without KD. Distillation is performed using both teachers, yielding eight teacher-student combinations. Cross-dataset generalization is assessed by training students on BBBC038 using TissueNet-cached SAM ViT-H predictions without teacher retraining. Across all experiments, preprocessing and optimization settings remain fixed; only the teacher, student backbone, and use of KD vary.

IV. RESULTS

A. Quantitative Results

Table I presents segmentation performance across all experimental conditions. The student models operate with 1.5M–27M parameters at inference compared to 632M for SAM ViT-H, achieving up to a 421× parameter reduction while requiring only a single input channel.

1) *Effect of Knowledge Distillation*: KD consistently improves performance over the baseline across all architectures. On TissueNet, SAM ViT-H distillation improves Dice by 13.05, 11.97, 12.05, and 12.07 points for Swin-Tiny, ResNet18, EfficientNet-B0, and MobileNetV3, respectively. The consistency of these gains across architectures spanning an order of magnitude in parameter count confirms that the benefits of distillation are largely independent of model capacity. CellSAM also improves performance over the baseline, although by a consistently smaller margin than SAM ViT-H, indicating that teacher quality directly affects distillation effectiveness.

2) *Effect of Student Capacity*: Larger student architectures achieve higher absolute performance for both baseline and distilled settings. On TissueNet with SAM ViT-H distillation, Dice scores range from 70.83 for MobileNetV3 (1.5M parameters) to 78.36 for Swin-Tiny (27M parameters), corresponding to a 7.53-point difference across an 18× range in model size. However, the relative gains from KD remain remarkably consistent across architectures (approximately 12 Dice points), suggesting that teacher supervision provides complementary semantic and boundary information regardless of student capacity. Notably, even the smallest student benefits substantially from distillation, supporting deployment in resource-constrained environments.

3) *Teacher Model Comparison*: SAM ViT-H consistently outperforms CellSAM as a teacher across all students and datasets. On TissueNet, SAM-distilled students exceed CellSAM-distilled students by 4.69–5.12 Dice points, reflecting the 7.79-point difference between the corresponding teacher oracles (89.12 vs. 81.33). This trend suggests that teacher oracle performance on the target domain is a stronger

TABLE I

SEGMENTATION PERFORMANCE COMPARISON ACROSS TEACHER MODELS, STUDENT ARCHITECTURES, AND DATASETS. RESULTS ARE AVERAGED OVER THREE INDEPENDENT RUNS AND REPORTED AS MEAN \pm STANDARD DEVIATION. BEST RESULT PER DATASET IN **BOLD**.

Dataset	Teacher	Student	Params	Input	Method	Dice	IoU	
TissueNet	SAM ViT-H	–	632M	2-ch	Teacher Oracle	89.12 \pm 1.21	81.21 \pm 1.50	
	CellSAM	–	635M	2-ch	Teacher Oracle	81.33 \pm 1.43	73.78 \pm 1.33	
	–	Swin-Tiny	27M	1-ch	Baseline	65.31 \pm 1.35	62.25 \pm 1.47	
	CellSAM	Swin-Tiny	27M	1-ch	Distilled	73.24 \pm 1.56	69.58 \pm 1.71	
	SAM ViT-H	Swin-Tiny	27M	1-ch	Distilled	78.36 \pm 1.44	73.29 \pm 1.38	
	–	ResNet18	11M	1-ch	Baseline	63.84 \pm 1.48	60.71 \pm 1.52	
	CellSAM	ResNet18	11M	1-ch	Distilled	71.12 \pm 1.62	67.24 \pm 1.66	
	SAM ViT-H	ResNet18	11M	1-ch	Distilled	75.81 \pm 1.45	71.06 \pm 1.53	
	–	EfficientNet-B0	5.3M	1-ch	Baseline	62.47 \pm 1.61	59.28 \pm 1.66	
	CellSAM	EfficientNet-B0	5.3M	1-ch	Distilled	69.63 \pm 1.74	65.81 \pm 1.79	
	SAM ViT-H	EfficientNet-B0	5.3M	1-ch	Distilled	74.52 \pm 1.51	69.84 \pm 1.63	
	–	MobileNetV3	1.5M	1-ch	Baseline	58.76 \pm 1.82	55.17 \pm 1.91	
	CellSAM	MobileNetV3	1.5M	1-ch	Distilled	66.18 \pm 1.88	61.75 \pm 1.95	
	SAM ViT-H	MobileNetV3	1.5M	1-ch	Distilled	70.83 \pm 1.79	65.94 \pm 1.87	
	BBBC038	–	Swin-Tiny	27M	1-ch	Baseline	80.19 \pm 1.43	77.42 \pm 1.37
		CellSAM	Swin-Tiny	27M	1-ch	Distilled	84.52 \pm 1.26	80.76 \pm 1.42
SAM ViT-H		Swin-Tiny	27M	1-ch	Distilled	87.44 \pm 1.28	83.54 \pm 1.59	
–		ResNet18	11M	1-ch	Baseline	78.14 \pm 1.49	74.91 \pm 1.45	
CellSAM		ResNet18	11M	1-ch	Distilled	82.37 \pm 1.41	78.65 \pm 1.52	
SAM ViT-H		ResNet18	11M	1-ch	Distilled	85.78 \pm 1.33	81.94 \pm 1.47	
–		EfficientNet-B0	5.3M	1-ch	Baseline	76.92 \pm 1.58	73.36 \pm 1.63	
CellSAM		EfficientNet-B0	5.3M	1-ch	Distilled	81.24 \pm 1.47	77.28 \pm 1.58	
SAM ViT-H		EfficientNet-B0	5.3M	1-ch	Distilled	84.81 \pm 1.36	80.84 \pm 1.51	
–		MobileNetV3	1.5M	1-ch	Baseline	74.28 \pm 1.73	70.52 \pm 1.78	
CellSAM		MobileNetV3	1.5M	1-ch	Distilled	79.13 \pm 1.66	75.21 \pm 1.74	
SAM ViT-H		MobileNetV3	1.5M	1-ch	Distilled	82.57 \pm 1.54	78.43 \pm 1.67	

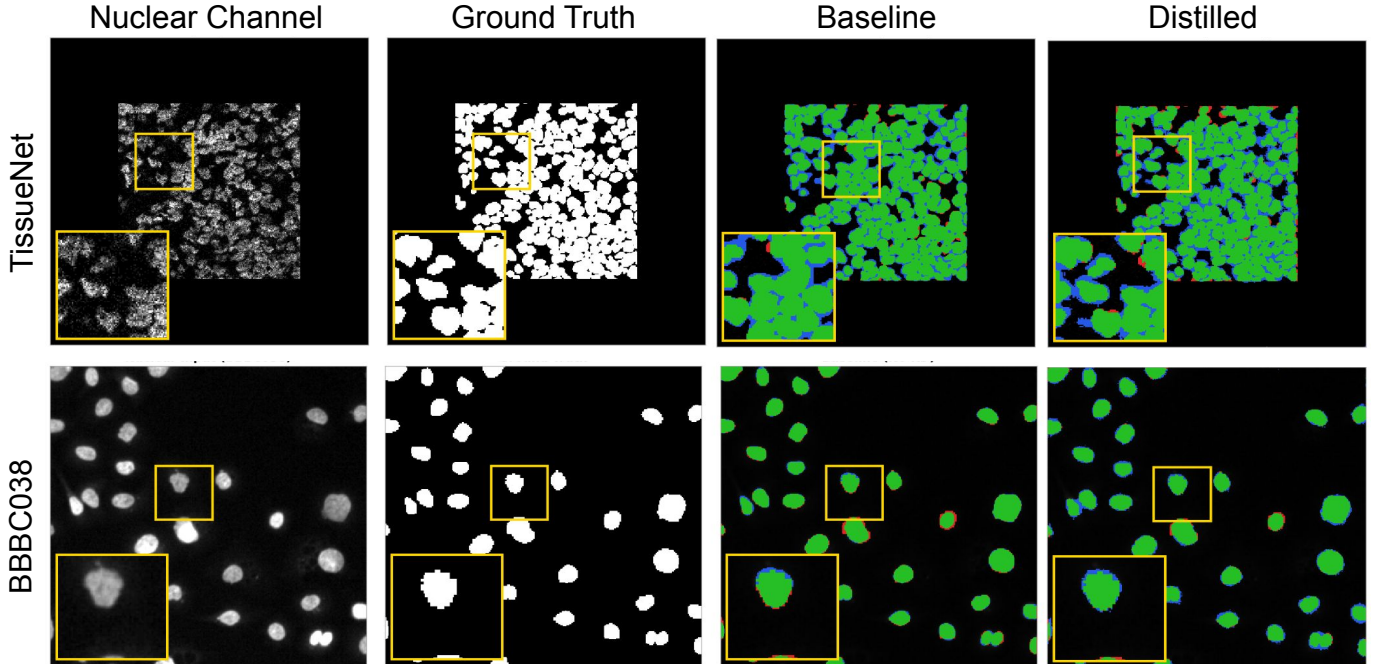


Fig. 3. Qualitative segmentation results on TissueNet validation set. Each row shows a different sample. Columns show nuclear channel input, ground truth mask, baseline prediction, and distilled prediction using SAM ViT-H as teacher. Color coding: ■ True Positive, ■ False Negative, ■ False Positive. Yellow boxes indicate magnified inset regions.

indicator of distillation quality than domain specialization alone.

4) *Cross-Dataset Results*: On BBBC038, SAM-distilled students improve over baselines by 7.25–8.29 Dice points

without teacher retraining, while CellSAM provides smaller but consistent gains of 4.33–4.85 points. These improvements demonstrate that teacher soft-targets capture transferable semantic representations that generalize across imaging conditions and tissue types. The consistent gains across all student architectures indicate that the proposed framework remains effective under cross-dataset distribution shifts.

Overall, the results establish three key findings. First, cross-modal KD consistently closes the modality gap, improving TissueNet performance by approximately 12 Dice points across all student architectures. Second, teacher quality strongly influences distillation effectiveness, with SAM ViT-H consistently producing stronger students than CellSAM. Third, the observed gains on BBBC038 demonstrate that the proposed framework generalizes across datasets without requiring teacher retraining, supporting practical deployment scenarios where multiplexed target-domain data may be unavailable.

B. Qualitative Results

Qualitative results for the best-performing configuration (SAM ViT-H teacher and Swin-Tiny student) are shown in Fig. 3. The top row presents TissueNet examples, while the bottom row shows cross-dataset results on BBBC038. The color-coded overlays indicate true positives (green), false negatives (red), and false positives (blue).

On TissueNet, the baseline model produces fragmented predictions with noticeable boundary errors, particularly in densely packed regions where nuclear signals alone are insufficient to delineate neighboring cells. In contrast, the distilled model recovers more coherent cell boundaries and reduces both false positives and false negatives. The zoomed regions further demonstrate that distillation is especially effective in crowded cellular areas, where membrane information available to the teacher provides additional structural guidance.

On BBBC038, segmentation is generally easier because nuclei are larger and more isolated. Nevertheless, the distilled model still produces cleaner boundaries and fewer segmentation errors than the baseline model. The consistent improvements observed across both datasets visually support the quantitative gains reported in Table I and indicate that the transferred knowledge remains effective despite the distribution shift between TissueNet and BBBC038.

V. CONCLUSION

This work presented a cross-modal knowledge distillation framework for tissue segmentation under missing-channel constraints. A frozen multiplexed teacher transfers information from nucleus and membrane channels to lightweight single-channel students. This enables accurate segmentation using only the nucleus channel during inference. Across four student architectures and two datasets, knowledge distillation consistently improved segmentation performance while reducing computational complexity. SAM ViT-H also produced stronger student performance than CellSAM. It suggests that teacher quality plays an important role in effective knowledge transfer. Cross-dataset results on BBBC038 further showed that the framework generalized well without requiring teacher

retraining. This highlights its potential for practical biomedical imaging applications where multiplexed data may not always be available. Future work will extend this framework to instance and panoptic segmentation, multi-teacher distillation, and additional modalities such as H&E histology and phase-contrast microscopy.

REFERENCES

- [1] E. Moen, D. Bannon, T. Kudo, W. Graf, M. Bhatt, and D. Van Valen, "Deep learning for cellular image analysis," *Nature Methods*, vol. 16, pp. 1233–1246, 2019.
- [2] O. Ronneberger, P. Fischer, and T. Brox, "U-Net: Convolutional networks for biomedical image segmentation," in *Medical Image Computing and Computer-Assisted Intervention (MICCAI)*. Springer, 2015, pp. 234–241.
- [3] N. F. Greenwald, G. Miller, E. Moen, A. Kong, A. Kagel, T. Dougherty, C. C. Fullaway, B. J. McIntosh, K. X. Leow, M. S. Schwartz *et al.*, "Whole-cell segmentation of tissue images with human-level performance using large-scale data annotation and deep learning," *Nature Biotechnology*, vol. 40, pp. 555–565, 2022.
- [4] G. Hinton, O. Vinyals, and J. Dean, "Distilling the knowledge in a neural network," *arXiv preprint arXiv:1503.02531*, 2015.
- [5] Y. Liu, K. Chen, C. Liu, Z. Qin, Z. Luo, and J. Wang, "Structured knowledge distillation for semantic segmentation," in *IEEE/CVF Conference on Computer Vision and Pattern Recognition (CVPR)*, 2019, pp. 2604–2613.
- [6] A. Kirillov, E. Mintun, N. Ravi, H. Mao, C. Rolland, L. Gustafson, T. Xiao, S. Whitehead, A. C. Berg, W.-Y. Lo, P. Dollar, and R. Girshick, "Segment anything," in *IEEE/CVF International Conference on Computer Vision (ICCV)*, 2023, pp. 4015–4026.
- [7] A. Dosovitskiy, L. Beyer, A. Kolesnikov, D. Weissenborn, X. Zhai, T. Unterthiner, M. Dehghani, M. Minderer, G. Heigold, S. Gelly, J. Uszkoreit, and N. Houlsby, "An image is worth 16x16 words: Transformers for image recognition at scale," *ArXiv*, vol. abs/2010.11929, 2020.
- [8] U. Israel, B. Bhatt, B. Bhatt, B. Bhatt *et al.*, "A foundation model for cell segmentation," *bioRxiv*, 2023, doi:10.1101/2023.11.17.567630.
- [9] Z. Liu, Y. Lin, Y. Cao, H. Hu, Y. Wei, Z. Zhang, S. Lin, and B. Guo, "Swin transformer: Hierarchical vision transformer using shifted windows," in *IEEE/CVF International Conference on Computer Vision (ICCV)*, 2021, pp. 10012–10022.
- [10] K. He, X. Zhang, S. Ren, and J. Sun, "Deep residual learning for image recognition," in *IEEE/CVF Conference on Computer Vision and Pattern Recognition (CVPR)*, 2016, pp. 770–778.
- [11] M. Tan and Q. Le, "EfficientNet: Rethinking model scaling for convolutional neural networks," in *International Conference on Machine Learning (ICML)*, 2019, pp. 6105–6114.
- [12] A. G. Howard, M. Sandler, G. Chu, L.-C. Chen, B. Chen, M. Tan, W. Wang, Y. Zhu, R. Pang, V. Vasudevan, Q. V. Le, and H. Adam, "Searching for mobilenetv3," *2019 IEEE/CVF International Conference on Computer Vision (ICCV)*, pp. 1314–1324, 2019.
- [13] J. C. Caicedo, A. Goodman, K. W. Karhohs, B. A. Cimini, J. Ackerman, M. Haghghi, C. Heng, T. Becker, M. Doan, C. McQuin, M. Rohban, S. Singh, and A. E. Carpenter, "Nucleus segmentation across imaging experiments: the 2018 Data Science Bowl," *Nature Methods*, vol. 16, pp. 1247–1253, 2019.
- [14] A. Kendall, Y. Gal, and R. Cipolla, "Multi-task learning using uncertainty to weigh losses for scene geometry and semantics," in *IEEE/CVF Conference on Computer Vision and Pattern Recognition (CVPR)*, 2018, pp. 7482–7491.
- [15] A. G. Howard, M. Zhu, B. Chen, D. Kalenichenko, W. Wang, T. Weyand, M. Andreetto, and H. Adam, "Mobilenets: Efficient convolutional neural networks for mobile vision applications," *ArXiv*, vol. abs/1704.04861, 2017.
- [16] J. Ma, Y. He, F. Li, L. Han, C. You, and B. Wang, "Segment Anything in medical images," *Nature Communications*, vol. 15, p. 654, 2024.
- [17] C. Poynton, *Digital Video and HD: Algorithms and Interfaces*, 2nd ed. Morgan Kaufmann, 2012.
- [18] W. Falcon *et al.*, "PyTorch Lightning," <https://github.com/Lightning-AI/pytorch-lightning>, 2019.
- [19] I. Loshchilov and F. Hutter, "Decoupled weight decay regularization," in *International Conference on Learning Representations (ICLR)*, 2019.